C. R. Mecanique 341 (2013) 171–180

Contents lists available at SciVerse ScienceDirect

Comptes Rendus Mecanique

www.sciencedirect.com

Combustion, flow and spray dynamics for aerospace propulsion

# Impact of flame base dynamics on the non-linear frequency response of conical flames

## *Impact de la dynamique de la base de la flamme sur la réponse fréquentielle non-linéaire d'une flamme conique*

Alexis Cuquel [a,b,*], Daniel Durox [a,b], Thierry Schuller [a,b]

[a] *CNRS, UPR 288, Laboratoire d'Energétique Moléculaire et Macroscopique, Combustion (EM2C), 92290 Châtenay-Malabry, France*
[b] *École Centrale Paris, 92290 Châtenay-Malabry, France*

ARTICLE INFO

*Article history:*
Available online 16 January 2013

*Keywords:*
Combustion dynamics
Flame transfer function
Flame base motion
Unsteady heat transfer

*Mots-clés :*
Dynamique de combustion
Fonction de transfert de flamme
Mouvement de la base de la flamme
Transfert de chaleur instationnaire

ABSTRACT

The response of laminar premixed conical flames to velocity disturbances is considered theoretically and experimentally with a focus on the impact of the flame base dynamics on the non-linear behavior of the Flame Transfer Function (FTF). Unsteady heat transfer between the flame base and the burner lip is considered to model the flame base response. Predictions for the flame base response $\Xi(\omega)$ and flame transfer function $F(\omega)$ are compared to measurements over a large range of frequencies. The non-linear behavior of the FTF phase is shown to result from a competition between velocity disturbances contributing to a regular increase of the phase lag with frequency and flame base oscillations leading to a saturation of the phase lag at high frequencies. Increasing the forcing level leads to an early saturation of the phase lag of the FTF at lower frequencies. This analysis demonstrates the important role of flame foot oscillations controlling the saturation of the FTF phase lag.



RÉSUMÉ

La réponse d'une flamme conique prémélangée soumise à des perturbations de vitesse est étudiée théoriquement et expérimentalement, en se concentrant sur l'impact de la dynamique du point d'accrochage sur le comportement non-linéaire de la Fonction de Transfert de Flamme (FTF). Cette réponse est modélisée en considérant le transfert de chaleur instationnaire entre le brûleur et la base de la flamme. Les prévisions concernant la réponse du point d'accrochage $\Xi(\omega)$ ainsi que la Fonction de Transfert de Flamme $F(\omega)$ sont comparées à des mesures pour différentes fréquences. On montre notamment que le comportement non-linéaire de la phase de la FTF résulte d'une compétition entre les effets dus aux perturbations de vitesse, induisant une augmentation regulière de la phase de la FTF, et du point d'accrochage de la flamme, résultant en une saturation de la phase de la FTF à hautes fréquences. Cette analyse montre ainsi le rôle important des oscillations de la base de la flamme, contrôlant la saturation de la phase de la FTF.



* Corresponding author at: CNRS, UPR 288, Laboratoire EM2C, 92290 Châtenay-Malabry, France.
*E-mail addresses:* alexis.cuquel@ecp.fr (A. Cuquel), daniel.durox@ecp.fr (D. Durox), thierry.schuller@ecp.fr (T. Schuller).

1631-0721/$ – see front matter 
http://dx.doi.org/10.1016/j.crme.2012.11.004

## 1. Introduction

Premixed combustors are often prone to thermo-acoustic instabilities, featuring a strong coupling between the flame dynamics and the combustion chamber acoustics. The flame response to incoming flow perturbations is one important element of this coupling. To predict such instabilities, low-order models are often used, based on the Flame Transfer Function (FTF) linking incoming flow perturbations to heat release rate disturbances. In perfectly premixed systems and in the absence of mixture composition disturbances, the flame responds solely to velocity modulations [1]. For small perturbations, the FTF may be defined by a gain $G$ and phase $\varphi$, both function of the angular frequency $\omega$ [2]:

$$F(\omega) = \frac{\tilde{\dot{Q}}_1/\dot{Q}_0}{\tilde{v}_1/v_0} = G(\omega)e^{i\varphi(\omega)} \tag{1}$$

where fluctuations are analyzed in the frequency space by expanding the flow variables as $a = a_0 + \tilde{a}_1 \exp(-i\omega t)$, $\tilde{\dot{Q}}_1$ and $\tilde{v}_1$ indicating fluctuations in heat release rate and velocity at the burner outlet respectively. One important issue is to determine the correct phase lag $\varphi(\omega)$ between incident disturbances and the resulting heat release rate perturbations. Small differences in the phase lag may have severe consequences on the stability of a combustor [3].

The case of laminar conical flames constitutes an interesting generic configuration, also found in a few industrial applications, where it is possible to obtain an analytical expression for the FTF [4–7]. It can be used to identify the main parameters controlling the flame response [1,8–12], or validate simulation tools by providing a reference case [13,14]. Many different models for the FTF were proposed including effects of the flow velocity, stretch and curvature of the flame front (see for example [15]), anchoring point dynamics (see for example [11,16]), but only a few were validated yet with detailed measurements [5,6,9]. This work aims at extending the identification of the main flow parameters controlling the response of conical flames submitted to velocity modulations. A new model is proposed taking into account the combined effects of flame wrinkles and flame foot disturbances induced by velocity perturbations. It is shown that this enables to describe the high frequency behavior of the flame response observed in experiments and that the contribution of the flame base motion constitutes an important saturation mechanism at high amplitudes.

It is well known that the main features of the flame response can be reproduced by including a better description of the mean and perturbed velocity fields [9,13]. Cuquel et al. [17] recently proposed an analytical model based on an incompressible convective velocity perturbation [9] leading to a better description of the FTF phase at low frequencies and in the intermediate frequency range. The model however features a regular phase increase at high frequencies, while experimental data often feature a saturation in this frequency range. This phenomenon can be observed when the flame is submitted to acoustic disturbances [17] or flame base oscillations [11]. The origin of this saturation is still unclear, even if recent elements point out the contribution of the flame base motion.

Many FTF analytical models assume a motionless flame base, while a few experiments indicate that this assumption must be released. Karimi et al. [12] showed that, for a conical flame stabilized on a burner radius $R = 12.5$ mm, the oscillation of the flame base diameter may reach 1 mm. Dowling [18] also considered a motion of the flame base to model the non-linear flashback of a V-flame stabilized on a central bluff body. Lee et al. [19] derived an expression for the FTF showing the respective contributions of velocity and flame base oscillations. The link between these quantities is however not addressed in their study. Kornilov et al. [11] designed an experiment where the motion at the flame base can be imposed to investigate its role and its effect on the FTF. In their data, the FTF phase often exhibits a saturation at high frequency, but this phenomenon is not investigated. They also showed that flame foot disturbances are convected along the flame front and that the perturbed flame front produces in feedback a velocity perturbation around it. This was also demonstrated by Birbaud et al. [10] when the flow is modulated by acoustic excitation and modeled by Baillot et al. [9] as an incompressible convected velocity disturbance. Schuller et al. [13] used this velocity model to reproduce numerically the FTF of conical flames that was shown to match well with measurements. More recently Cuquel et al. [17] proposed an analytical expression of the corresponding FTF. There has been however so far no attempt to model the FTF of single conical flame including effects of the flame base motion with detailed experimental validations.

In this article, the link between flame base disturbances and their contributions to the FTF is derived analytically in Section 1. A model is then proposed in Section 2 for the motion of the flame foot by considering unsteady heat and mass transfers between the flame base and burner rim. Predictions from these models are then compared to experimental results in Section 3. It is shown that this new description enables to determine the saturation level of the FTF phase lag at high frequencies. It is finally shown that this saturation is promoted when the forcing level is increased indicating that the motion of the flame base is an essential feature of the non-linear conical flame frequency response.

## 2. Theoretical analysis

Axisymmetric premixed laminar conical flames submitted to flow rate modulations are considered in this study as represented schematically in Fig. 1. The following theoretical developments make use of the G-equation to model the shape of the perturbed flame front and to estimate the FTF. The flame front is considered as an infinitely thin interface separating

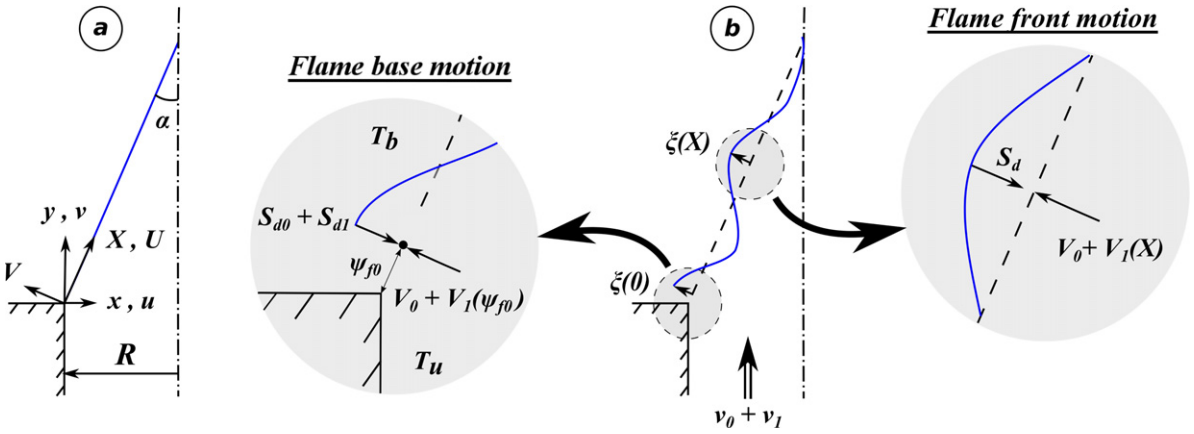


**Fig. 1.** Schematic of the configuration investigated. (a) Steady conical flame along with the different frames used in this article. (b) Acoustically perturbed conical flame, with a focus on the flame base region and the flame front displacement far from the burner.

the fresh and burnt gases, which is modeled by the iso-level $G(\mathbf{x}, t) = 0$ of the scalar $G$-field. Considering a constant flame displacement speed $S_d$ and the flow velocity $\mathbf{v}$ at the flame interface, the G-equation writes:

$$\frac{\partial G}{\partial t} + \mathbf{v} \cdot \nabla G = S_d |\nabla G| \tag{2}$$

The analysis is limited to an axial mean flow $\mathbf{v}_0 = (0, v_0)$ and small velocity disturbances $(u_1, v_1)$ compared to the mean velocity. In the burner frame, the velocity writes:

$$\mathbf{v}(\mathbf{x}, t) = u_1(\mathbf{x}, t)\mathbf{e_x} + \big(v_0 + v_1(\mathbf{x}, t)\big)\mathbf{e_y} \tag{3}$$

It is also interesting to write these velocity components in a frame attached to the flame front:

$$\mathbf{V}(\mathbf{X}, t) = \big(U_0 + U_1(\mathbf{X}, t)\big)\mathbf{e_X} + \big(V_0 + V_1(\mathbf{X}, t)\big)\mathbf{e_Y} \tag{4}$$

where $U_0 = v_0 \cos\alpha$ is the mean flow velocity component tangential to the flame front, $V_0 = v_0 \sin\alpha$ is the mean flow velocity component normal to the flame front and $\alpha$ is the flame tip half-angle. Following [6], the G-equation expressed in the flame frame reduces to:

$$\frac{\partial \xi}{\partial t} + U_0 \frac{\partial \xi}{\partial X} = V_1(X, t) \tag{5}$$

where $\xi(X, t) = \tilde{\xi}(X)e^{-i\omega t}$ is a harmonic perturbation of the flame front position normal to its steady position and $V_1(X, t)$ is the normal velocity perturbation along the steady flame front $Y = 0$. The solution of this equation is given by the telegraph integral [8,20,21]:

$$\tilde{\xi}(X) = \frac{e^{iKX}}{U_0} \int_0^X \tilde{V}_1(X') e^{-iKX'}\, \mathrm{d}X' + \tilde{\xi}(0) e^{iKX} \tag{6}$$

where $K = \omega/U_0$ is the wavenumber associated to the convection of flame front wrinkles along the steady flame front and $\tilde{\xi}(0)$ is the flame front displacement at the flame base $X = 0$.

The latter equation features two main contributions to flame wrinkling. The first term on the right hand side of Eq. (6) indicates that wrinkles produced at the flame base are convected along the flame front. The second term describes how velocity disturbances normal to the steady flame front produce wrinkles that propagate along the flame front. These two mechanisms contribute to the FTF linking heat release rate disturbances $\tilde{\dot{Q}}_1$ to velocity perturbations $\tilde{v}_1$ at the burner outlet:

$$F(\omega) = \frac{\tilde{\dot{Q}}_1 / \dot{Q}_0}{\tilde{v}_1 / v_0} = F_A(\omega) + F_B(\omega) \tag{7}$$

where $F_A$ and $F_B$ stand for velocity and flame base contributions to the FTF respectively. The first contribution $F_A(\omega)$ was already extensively investigated. It was shown that it is a function $F_A(\omega_*, \alpha)$ of the flame angle $\alpha$ and the reduced frequency $\omega_* = \omega R/(S_d \cos\alpha)$ [5,6,17,20]. The second contribution $F_B(\omega)$ resulting from the flame base motion is less documented [19]. It is considered here in more details.

The steady flame surface area is given by $A_0 = \pi R^2 / \sin\alpha$, while infinitesimal first order flame surface area disturbances $\mathrm{d}\tilde{A}_1$ in the $(X, Y)$ flame frame are given by:

$$\mathrm{d}\tilde{A}_1 = 2\pi \tilde{r}_1(X)\, \mathrm{d}l \tag{8}$$

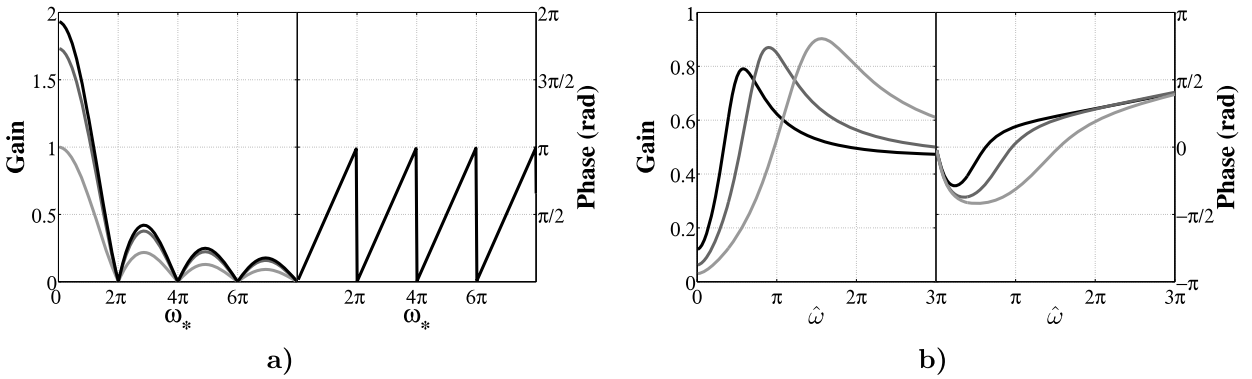


**Fig. 2.** (a) Transfer function $F_C(\omega_*, \alpha)$ plotted as a function of reduced frequency $\omega_*$ for different flame tip half-angles $\alpha = \pi/12$ (black), $\pi/6$ (dark grey), and $\pi/3$ (light grey). (b) Transfer function $\Xi(\hat{\omega}, \Psi_f, \omega_*, \alpha)$ plotted as a function of reduced frequency $\hat{\omega}$ for different dimensionless stand-off distances $\Psi_f = 1.36$ (black), 1.06 (dark grey), and 0.76 (light grey). The following values for the flame half-tip angle $\alpha = 0.28$ rad, the Zeldovich number $Ze = 10.2$, and the dimensionless thermal flame thickness $\delta_* = 0.0372$ were used here to obtain the curves plotted in (b).

where $dl$ is the infinitesimal length of the perturbed flame front. A local linear approximation gives $\tilde{r}_1(X) = \tilde{\xi}(X)\cos\alpha$ and $dl = dX$ to the first order. Considering now only the contribution to flame base disturbances in Eq. (6), one obtains:

$$\tilde{A}_{1B} = 2\pi \int_0^L \tilde{\xi}(X)\cos\alpha \, dX = 2\pi \cos\alpha \frac{e^{iKL} - 1}{iK}\tilde{\xi}(0) \tag{9}$$

which directly yields the sought flame transfer function component $F_B$:

$$F_B(\omega) = \frac{\tilde{A}_{1B}/A_0}{\tilde{v}_1/v_0} = \frac{\tilde{A}_{1B}/A_0}{\tilde{\xi}(0)/R}\frac{\tilde{\xi}(0)/R}{\tilde{v}_1/v_0} = F_C(\omega_*, \alpha)\Xi(\omega) \tag{10}$$

where

$$F_C(\omega_*, \alpha) = 2\cos\alpha \frac{e^{i\omega_*} - 1}{i\omega_*} \quad \text{with } \omega_* = \frac{\omega R}{S_d \cos\alpha} \quad \text{and} \quad \Xi(\omega) = \frac{\tilde{\xi}(0)/R}{\tilde{v}_1/v_0} \tag{11}$$

Equation (10) shows how small displacements at the flame base are filtered by the flame and produce heat release rate perturbations. The frequency response of the flame base motion with respect to velocity disturbances is represented here by $\Xi(\omega)$ as a function of the forcing frequency. Flame displacements at the base are then convected along the flame front and their contribution to heat release rate perturbations is described by the filter $F_C(\omega_*, \alpha) = G_c(\omega_*, \alpha)\exp(i\varphi_c(\omega_*))$ plotted in Fig. 2(a) with respect to the reduced frequency $\omega_*$ for different values of the flame tip half-angle $\alpha = \pi/3$, $\pi/6$ and $\pi/12$. The gain $G_c$ is a low-pass filter with decreasing amplitudes for increasing flame angles $\alpha$. The unwrapped phase $\varphi_c$ is independent of the flame angle and oscillates with respect to the forcing frequency between 0 and $\pi$, without any values between $\pi$ and $2\pi$. It does not feature a convective behavior, which would result in a regular increase of the phase with the reduced frequency. The remaining problem is to model the flame foot displacement induced by velocity disturbances at the burner outlet to determine $\Xi(\omega)$. This issue is addressed in the next section.

## 3. Modeling the flame base frequency response

The motion of planar premixed flames stabilized close to solid walls and submitted to acoustic perturbations has already been studied in various configurations [16,22]. It was shown that a planar flame close to a solid boundary can be perturbed in two ways. First, acoustic velocity perturbations can produce regular flame front displacements. Then, these perturbations of the flame position close to a solid boundary may in turn lead to a resonant coupling in certain circumstances [22]. Heat transfer from the flame to the burner is here of significant importance. The following analysis relies on the transport of total enthalpy $h_t = \Delta h_f^0 Y_f + c_p T$ disturbances between the flame front and the burner tip, where $\Delta h_f^0$ is the heat value per unit mass of fuel, $Y_f$ is the fuel mass fraction in the mixture, $c_p$ is the mixture specific heat at constant pressure and $T$ is the mixture temperature.

The presumed scenario is the following [22]. Fluctuations of the flame front location induce enthalpy disturbances that are transported by both convection and diffusion processes, from the burner lip to the flame front where they induce temperature fluctuations. When these disturbances reach the flame front, they induce in turn perturbations in flame speed producing a displacement of the flame front. These phenomena can couple and lead to resonance when the enthalpy disturbance wavelength is of the order of $4\psi_{f0}$ [22,23] where $\psi_{f0}$ stands for the steady flame stand-off distance above the

burner. It is possible to model the transfer function linking flame displacement speed perturbations $\tilde{S}_{d1}$ and acoustic velocity disturbances $\tilde{V}_1(X=\psi_{f0})$ at the flame base [22]:

$$\mathcal{A}(\hat{\omega}, Ze, \Psi_f) = \frac{\tilde{S}_{d1}}{\tilde{V}_1(X=\psi_{f0})} = \left[1 - \frac{i\hat{\omega}}{Ze}\sinh(\Psi_f)\exp\left(\Psi_f(1-i\hat{\omega})^{1/2}\right)\right]^{-1} \tag{12}$$

where

$$\hat{\omega} = 4\omega\frac{\delta}{S_{d0}} = 4\delta_*\omega_*, \quad \delta_* = \delta\frac{\cos\alpha}{R}, \qquad Ze = \frac{T_a}{T_b}\frac{T_b - T_u}{T_b} \quad \text{and} \quad \Psi_f = \frac{\psi_{f0}}{2\delta} = \frac{1}{2}\log\left(\frac{T_{\text{ad}} - T_u}{T_{\text{ad}} - T_b}\right) \tag{13}$$

In these expressions $\omega$ denotes the angular frequency of the acoustic forcing, $\delta$ indicates the thermal flame thickness, $S_{d0}$ is the steady flame displacement speed, $Ze$ is the Zeldovich number, $T_a$ is the activation temperature, $T_b$ is the steady burnt gas temperature, $T_u$ is the steady fresh mixture gas temperature, also taken here as the burner lip temperature, $\psi_{f0}$ corresponds to the steady flame stand-off distance above the burner (see Fig. 1), and $T_{\text{ad}}$ is the adiabatic flame temperature.

By taking into account these burning velocity disturbances, the motion of the flame foot of a conical flame can be investigated using a local kinematic description. The flame base being close to the burner wall where the mean flow velocity is reduced, the convective term in the G-equation (Eq. (5)) can be neglected:

$$\frac{\partial\xi(0)}{\partial t} = V_1(\psi_{f0}, t) - S_{d1}(t) \tag{14}$$

where $V_1(\psi_{f0}, t)$ indicates the velocity perturbation normal to the flame front at the flame base $X=\psi_{f0}$ and $S_{d1}(t)$ denotes disturbances of the flame displacement speed at the same location. Using the Fourier transform of Eq. (14), one obtains an expression for the flame base motion transfer function:

$$\Xi(\omega) = -\frac{v_0}{i\omega R}\left(1 - \frac{\tilde{S}_{d1}}{\tilde{V}_1(\psi_{f0})}\right)\frac{\tilde{V}_1(\psi_{f0})}{\tilde{v}_1} \tag{15}$$

To close the problem, the remaining difficulty is to specify the relation linking the normal velocity perturbation $\tilde{V}_1(\psi_{f0})$ at the flame base $X=\psi_{f0}$ to the axial velocity modulation $\tilde{v}_1$ at the burner outlet. It is known that the perturbed velocity field takes the form of an incompressible convective wave [9,10,13]. Baillot et al. [9] derived an expression that has been adapted in the $(X, Y)$ frame in [17]:

$$\frac{\tilde{V}_1(\psi_{f0})}{\tilde{v}_1} = \sin\alpha\left(1 - \frac{ik_*}{2}\left(1 - \frac{\psi_{f0}}{L}\right)\right)\exp\left(ik_*\frac{\psi_{f0}}{L}\right) \tag{16}$$

where $L = R/\sin\alpha$ is the steady flame front length and $k_* = \omega H/v_0 = \omega_*\cos^2\alpha$ denotes the wavenumber associated to flow perturbations convected along the axial direction. By combining Eqs. (15) and (16), one finally obtains the desired expression linking perturbations at the flame base due to incoming velocity disturbances:

$$\Xi(\hat{\omega}, \Psi_f, \omega_*, \alpha) = \frac{\tilde{\xi}(0)/R}{\tilde{v}_1/v_0} = -\frac{1 - \mathcal{A}(\hat{\omega}, \Psi_f)}{i\omega_*\cos\alpha}\left(1 - \frac{ik_*}{2}\left(1 - \frac{\psi_{f0}}{L}\right)\right)\exp\left(ik_*\frac{\psi_{f0}}{L}\right) \tag{17}$$

The transfer function $\Xi$ is mainly a function of the reduced frequencies $\hat{\omega}$, comparing the acoustic time scale to the flame thermal diffusion time scale, and $\omega_*$, comparing the acoustic time scale to the mean flow time scale. In this description, two other parameters need also to be taken into account. They correspond to $\Psi_f$, the ratio of the flame stand-off distance to the flame thermal thickness, and the flame tip half-angle $\alpha$.

Predictions for $\Xi(\hat{\omega}, \Psi_f, \omega_*, \alpha)$ are plotted in Fig. 2(b) as a function of $\hat{\omega}$, in terms of gain and phase for different flame foot dimensionless stand-off distances $\Psi_f$ and a fixed Zeldovich number $Ze = 10.2$ [24]. The response corresponds to a frequency band-pass filter with a resonance-like behavior in the intermediate range of reduced frequencies $\hat{\omega}$. The gain decreases to zero as the reduced frequency $\hat{\omega}$ is further increased. The phase lag exhibits a decrease at low frequencies, before increasing again and saturating at a constant level at high reduced frequencies $\hat{\omega}$. The peak of this transfer function strongly depends on the dimensionless stand-off distance $\Psi_f$. The resonance frequency shifts to higher frequencies as $\Psi_f$ decreases. All other parameters remaining constant, a drop in the flame stand-off distance corresponds to a shorter resonance wavelength and a peak frequency shifted to higher frequencies.

This analysis shows that the contribution $F_B(\omega) = F_C(\omega_*, \alpha)\Xi(\hat{\omega}, \Psi_f, \omega_*, \alpha)$ from wrinkles induced by the flame base motion to the FTF $F(\omega)$ features a saturation of the phase lag at high frequencies originating from $\Xi(\hat{\omega}, \Psi_f, \omega_*, \alpha)$ which is modulated by the oscillation of $F_C(\omega_*, \alpha)$. It is also known that the phase lag of the contribution $F_A(\omega)$ resulting from flame wrinkles induced by acoustic forcing is regularly increasing with the forcing frequency [6,17], except at very high flame tip half-angles. The model developed in this study $F(\omega) = F_A(\omega_*, \alpha) + F_B(\omega_*, \alpha, \hat{\omega}, \Psi_f)$ shows that the phase lag is linearly increasing at low and intermediate frequencies while saturating at high frequencies when the gain of $F_B$ overcomes the gain of $F_A$. An experimental validation of these predictions is proposed in the next section.

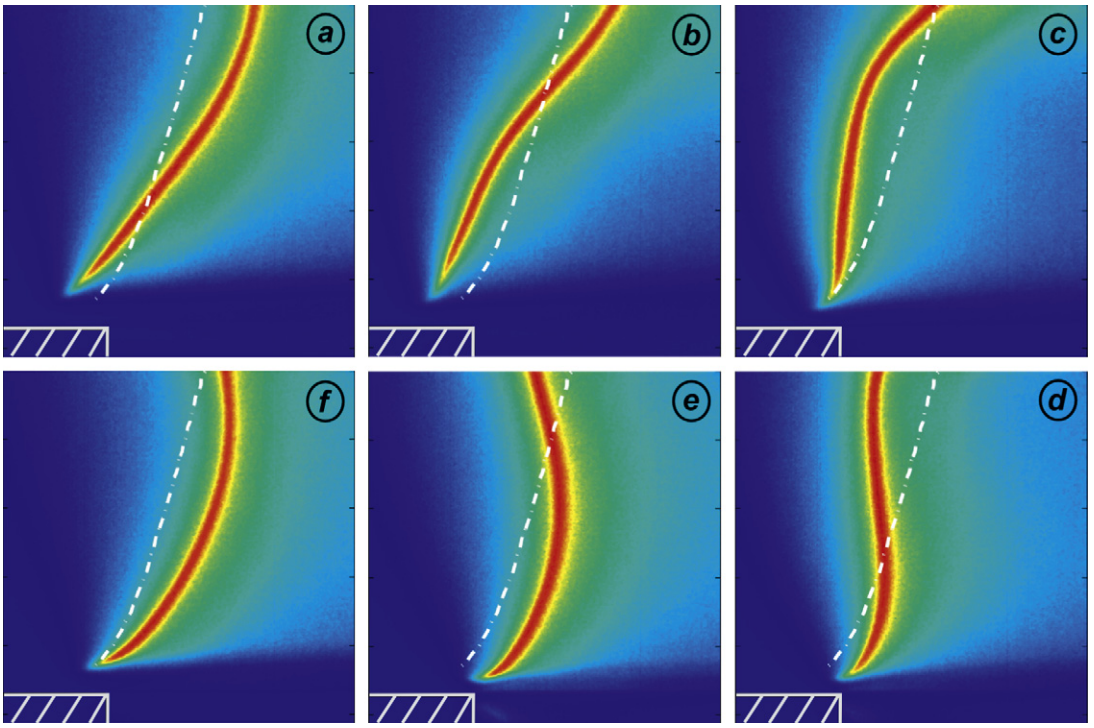


**Fig. 3.** Flame base motion at six regularly spaced phases during a modulation cycle for a forcing frequency $f = 100$ Hz and a rms velocity fluctuation level $\tilde{v}_{1\,\mathrm{rms}}/v_0 = 0.1$. The steady flame position is indicated as white dashed-dotted lines. The burner edge is represented in white in the bottom left part of the images.

## 4. Experimental investigation

### 4.1. Experimental setup

The configuration studied here features a cylindrical feeding manifold equipped with a laminarization grid and a convergent nozzle used to reduce remaining turbulent fluctuations and to get a nearly uniform top-hat velocity profile at the burner exit. The burner outlet is circular with a radius $R = 11$ mm. The bottom of the burner is equipped with a loudspeaker to produce harmonic acoustic disturbances. In these experiments, methane and air are perfectly premixed before entering the manifold with a fixed equivalence ratio $\phi = 1.03$, which sets the laminar burning velocity to $S_L = 0.39\ \mathrm{m\,s^{-1}}$ and the mean flow velocity to $v_0 = 1.56\ \mathrm{m\,s^{-1}}$ at the burner outlet.

The loudspeaker is driven by a harmonic signal generated with the Labview software, with a sampling frequency of $f_s = 4096$ Hz, connected to a HiFi-amplifier. It produces a harmonic velocity modulation at the burner exit, which is measured by Laser Doppler Velocimetry (LDV) at the base of the flame, 2 mm above the burner exit on the burner axis. A photodiode equipped with an OH* filter records the chemiluminescence emission from the flame, which is proportional to the heat release rate in this case [5,25]. The forcing signal, velocity and heat release rate time series are all recorded at once with a National Instrument analog-to-digital converter board controlled by the Labview software. The sampling frequency is also 4096 Hz. These signals are further post-processed by cross- and auto-correlations to determine the FTF as a function of the angular frequency $\omega$ for a fixed velocity modulation level:

$$F(\omega) = \frac{\tilde{\dot{Q}}_1/\dot{Q}_0}{\tilde{v}_1/v_0} \tag{18}$$

An intensified CCD camera is also used to take snapshots of the steady and perturbed flames. A TTL signal is generated with the same period as the Labview harmonic forcing signal to trigger the camera and obtain phase conditioned average images. The flame motion was decomposed in 18 successive phases of the forcing period. The signal to noise ratio was improved by taking more than a hundred snapshots for each phase of the modulation cycle investigated. The motion of the flame base was determined by zooming in the region near the burner outlet. The flame front location was firstly detected by identifying the maximum pixel value on every horizontal lines of the phase conditioned average images. The flame base was then identified by detecting the location where the light intensity is equal to a threshold value which is set to 60% of the maximum pixel value over the whole image. A sensitivity analysis to the threshold level was conducted and yielded the same type of results as the ones presented here. The flame foot motion was then determined by measuring the horizontal

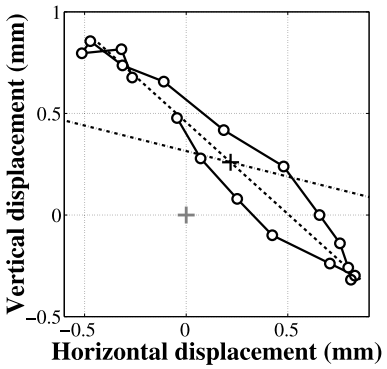


**Fig. 4.** Flame base motion for a modulation at $f = 100$ Hz and $\tilde{v}_{1\,\mathrm{rms}}/v_0 = 0.1$. (grey +) Steady flame base location. (black +) Mean location of the flame base displacement. (black line with -○-) Flame base motion determined experimentally. (black dashed lines) Main direction of the flame base motion determined experimentally $\alpha_{\mathrm{base}}$. (black dashed-dotted lines) Theoretical line normal to the flame front, defined by $\alpha = \arcsin(S_{d0}/v_0)$.

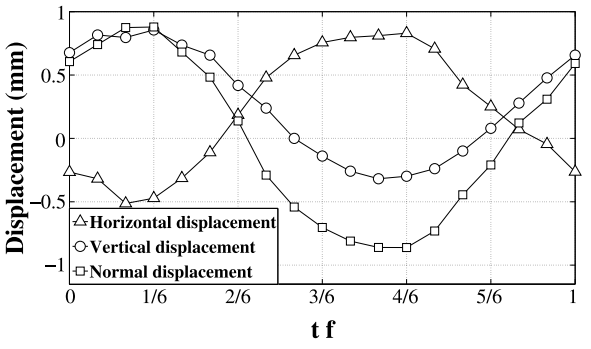


**Fig. 5.** Flame base displacement versus dimensionless time for a modulation at $f = 100$ Hz and $\tilde{v}_{1\,\mathrm{rms}}/v_0 = 0.1$. The horizontal (△) and vertical (○) displacements with respect to the steady flame location are represented, as well as the displacement in the normal direction (□) with respect to the flame front.

and vertical displacement components $(x_1, y_1)$ with respect to its mean position during the cycle. The harmonic normal displacement signal $\xi_1^0(\theta) = |x_1(\theta) + iy_1(\theta)|$ with respect to the mean flame front direction can then be computed and the flame angle $\alpha_{\mathrm{base}} = -\arctan(\tilde{y}_1/\tilde{x}_1)$ with respect to the flow direction at the flame origin can be determined. These data were used to determine the transfer function $\Xi(\omega)$ by cross- and auto-correlation of the flame base motion signal $\tilde{\xi}(0)$ and the velocity signal $\tilde{v}_1$ measured by LDV at the burner outlet:

$$\Xi(\omega) = \frac{\tilde{\xi}(0)/R}{\tilde{v}_1/v_0} \tag{19}$$

This transfer function was measured for different forcing frequencies and perturbation levels.

### 4.2. Analysis of the flame base motion

Six phase conditioned average images, separated by a constant phase lag, are presented in Fig. 3 over a modulation cycle for a forcing frequency $f = 100$ Hz and a velocity perturbation level $\tilde{v}_{1\,\mathrm{rms}}/v_0 = 0.1$, where $v_{1\,\mathrm{rms}}$ denotes the root mean square velocity fluctuation at the burner outlet. The steady flame position is also plotted in these figures as dashed-dotted white lines to provide a reference. These images clearly show that the flame base is not motionless, but undergoes a periodic motion around its steady position. These perturbations are then convected along the flame front. Figure 4 plots the displacement of the flame foot around its mean position during one forcing period. This motion features a periodic behavior with the same oscillation frequency as the velocity modulation. The motion from the flame base is roughly oriented along particular direction, supporting the fact that the perturbations at the flame base can effectively be well described only by a displacement normal to the mean flame front. It was also found that the mean and steady flame front positions coincide well.

These observations are further supported by Fig. 5 where the flame base displacement is plotted with respect to the phase of the forcing signal. The three curves represent the horizontal, vertical and normal to the flame front displacement components. They all feature a periodic motion which is nearly a harmonic function of time. The amplitude of this displacement is of the order of 1 mm, a value which is consistent with other studies for the same forcing level [12]. The measured amplitudes of the horizontal and vertical displacements of the flame foot are then used to compute the principal direction of the flame foot motion. This information also enables to determine the slope of the mean flame front direction near the flame base, defined by $\alpha_{\mathrm{base}}$. This direction of the flame foot motion is indicated as black dashed lines in Fig. 4. The normal direction with respect to the theoretical flame front direction defined by the half-angle at the flame tip $\alpha = \sin^{-1}(S_d/v_0)$ is also indicated as black dashed-dotted lines for comparison. Predictions largely deviate from measurements because the flame angle at the flame base differs from the one at the flame tip. The angle at the flame base is determined by a competition between the flow velocity and the flame burning velocity at this location. The burning velocity at the flame base is modified by heat losses to the burner rim, while the flow velocity near the burner edge lies in the jet boundary layer and takes small values. These effects combine and modify the flame angle with respect to its value far from the burner edges [26]. This phenomenon is also visible in the images of the steady flame, where the flame front is slightly bent close to the burner edge (dashed-dotted lines in Fig. 3).

Measurements of the flame base motion are now post-processed to determine the transfer function $\Xi_{exp}(\omega)$. These data can be compared with predictions from Eq. (17) as a function of the forcing frequency. The following parameters were used to compute $\Xi(\hat{\omega})$: $T_{\mathrm{ad}} = 2234$ K, $T_b = 2000$ K, $T_u = 300$ K, $T_a = 24\,000$ K, $S_{d0} = 0.39\ \mathrm{m\,s^{-1}}$, $\delta = 0.0005$ m, $R = 0.011$ m and $v_0 = 1.56\ \mathrm{m\,s^{-1}}$ for a stoichiometric methane/air flame. The flame stand-off distance was determined using images of the steady flame $\psi_{f0} = 0.9$ mm (Fig. 3). This set of parameters correspond to dimensionless values $Ze = 10.2$ [24], $\delta_* = 0.037$

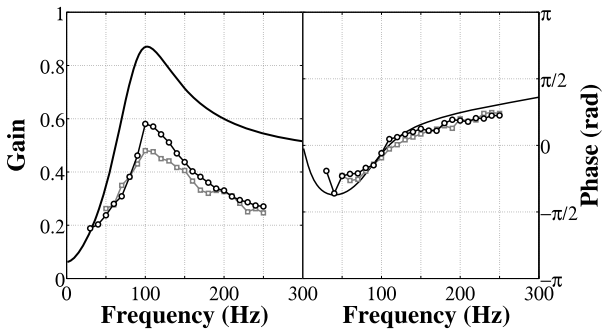


**Fig. 6.** The transfer function $\Xi(\omega)$ gain (left) and phase (right) as a function of the forcing frequency. The theoretical transfer function (black curve) is compared to measurements for $\tilde{v}_{1\,\mathrm{rms}}/v_0 = 0.05$ (grey curve with square symbols) and $\tilde{v}_{1\,\mathrm{rms}}/v_0 = 0.10$ (black curve with circle symbols).

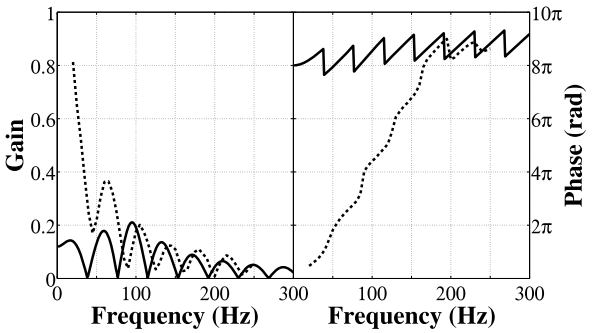


**Fig. 7.** Flame transfer function component $F_B(\omega)$ gain (left) and phase (right) as a function of the forcing frequency. The theoretical contribution $F_B(\omega)$ (black curve) is compared to measurements of the flame transfer function $F(\omega)$, for $\tilde{v}_{1\,\mathrm{rms}}/v_0 = 0.04$ (black dashed curve).

and $\Psi_f = 1.06$. Measurements were conducted for two velocity modulation levels $\tilde{v}_{1\,\mathrm{rms}}/v_0 = 0.05$ and $\tilde{v}_{1\,\mathrm{rms}}/v_0 = 0.10$ over the frequency range 30–250 Hz with a frequency resolution of 10 Hz. Results are presented in Fig. 6. Experimental data for the gain show a resonance-like behavior which frequency lies around 100 Hz and amplitude reaches almost 0.6. Data for the two modulation levels collapse on the same curve except in the region near the peak value of the gain which slightly increases with the perturbation level. This observation is in agreement with previous measurements [12], where the mean value of the flame base diameter was found equal to its steady value up to a very high forcing level $\tilde{v}_1/v_0 \simeq 1$, while the dimensionless flame base diameter modulation scaled linearly with the perturbation level $\tilde{v}_1/v_0$. The phase lag in Fig. 6 decreases first with increasing frequencies before reaching an almost constant value for frequencies higher than 170 Hz. This behavior is in good agreement with predictions, except that the predicted gain exceeds by far measurements. The global behavior is however well retrieved including the correct peak frequency for the gain of the flame base response. More importantly, the phase lag is well retrieved by the model.

It is now possible to examine the evolution of the phase lag at high frequency. Expressions from Eqs. (11) and (17) for $F_C(\omega)$ and $\Xi(\omega)$ are combined and used to estimate the contribution $F_B(\omega) = F_C(\omega)\Xi(\omega)$ to the conical flame response. Results are plotted in Fig. 7, where the prediction for $F_B(\omega)$ (black solid line) is compared to the FTF $F(\omega)$ (black dashed lines) determined experimentally. The phase lags of the functions $F_B$ and $F$ match well at high frequency featuring both a saturation, while their gains exhibit the same behavior in this frequency range. This demonstrates that saturation of the FTF phase lag at high frequency may be predicted by taking into account the motion of the flame foot. This motion at the flame base determines the high frequency behavior of the flame response to velocity perturbations.

It is finally interesting to examine the evolution of the saturation frequency. This quantity can be defined, for a fixed perturbation level, as the lowest frequency where the FTF phase starts to be almost constant and looses its convective behavior. The saturation frequency is for example equal to $f_{\mathrm{sat}} = 160$ Hz in Fig. 7. It has recently been shown that for conical flames submitted to flow rate modulations, the saturation frequency decreases with the velocity forcing amplitude at the burner outlet, as seen in Fig. 8, adapted from [2]. In these experiments, it was found that $f_{\mathrm{sat}} = 120$ Hz for $v_1/v_0 = 0.07$ and $f_{\mathrm{sat}} = 80$ Hz for $v_1/v_0 = 0.14$. This mechanism can be explained by the following scenario. The gain of the contribution $F_A$ to the FTF resulting from velocity disturbances reduces with the forcing level [2,3], while it was shown in this study and in [12] that the flame foot motion features a regular amplitude increase with the forcing level. This indicates that the relative contribution $F_B$ due to the flame foot motion to the FTF increases compared to the contribution $F_A$ resulting from velocity disturbances when the perturbation level increases. As $F_A$ dominates the flame response at low frequencies and $F_B$ determines the high frequency behavior of the flame response, saturation of the phase lag occurs at lower forcing frequencies when the forcing level is increased.

## 5. Conclusion

Improved expressions for the FTF of conical flames submitted to velocity disturbances were derived in this study by including in the description the motion of the flame base. The frequency response of this motion was modeled by taking into account unsteady heat losses between the flame base and burner rim and the structure of the perturbed velocity field in the fresh stream. This led to an analytical expression of the frequency response of the flame base motion. An experimental validation of these predictions was carried out. The motion at the flame base was analyzed with phase conditioned average images under acoustic forcing enabling to determine its frequency response when the forcing frequency and the perturbation level are modified. Predictions compare well with these experimental data. The gain is slightly over-predicted, but the phase lag is correctly retrieved and exhibits a saturation at high frequencies. This saturation of the phase lag is also observed on the FTF component $F_B(\omega)$ linked to the flame base motion. It was shown that this new contribution to the FTF becomes predominant at high frequency and determines the saturation of the phase lag at high frequency. It was also shown that this phenomenon shifts to lower frequencies when the perturbation level at the burner outlet increases,

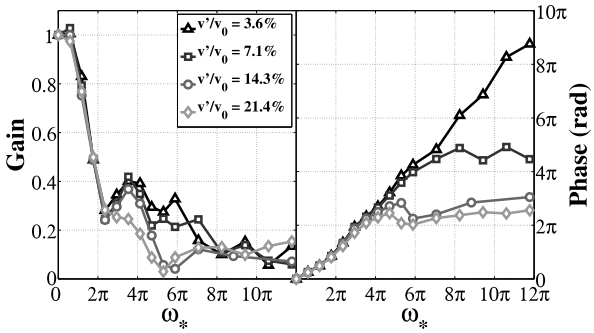


**Fig. 8.** Flame transfer function of a conical flame $v_0 = 1.96\ \mathrm{m\,s^{-1}}$ and $\phi = 1.08$ plotted as a function of the reduced frequency $\omega_*$ for different perturbation levels. Adapted from Fig. 3 in [2].

emphasizing the important role of the flame foot dynamics in the non-linear description of the flame frequency response to velocity disturbances.

## Acknowledgements

The research leading to these results has received funding from the European Community's Seventh Framework Programme (FP7/2007–2013) under Grant Agreement #ACP8-GA-2009-234009. This is part of the 4-year KIAI project started in May 2009, which is a European initiative financed under the FP7 and addresses innovative solutions for the development of new combustors in aero-engines. It aims at providing low NOx methodologies to be applied to design these combustors.

## References

[1] S. Ducruix, T. Schuller, D. Durox, S. Candel, Combustion dynamics and instabilities: Elementary coupling and driving mechanisms, Journal of Propulsion and Power 19 (2003) 722–734.
[2] D. Durox, T. Schuller, N. Noiray, S. Candel, Experimental analysis of nonlinear flame transfer functions for different flame geometries, Proceedings of the Combustion Institute 32 (1) (2009) 1391–1398.
[3] N. Noiray, D. Durox, T. Schuller, S. Candel, A unified framework for nonlinear combustion instability analysis based on the flame describing function, Journal of Fluid Mechanics 615 (1) (2008) 139–167.
[4] M. Fleifil, A.M. Annaswamy, Z.A. Ghoneim, A.F. Ghoniem, Response of a laminar premixed flame to flow oscillations: A kinematic model and thermoacoustic instability results, Combustion and Flame 106 (4) (1996) 487–510.
[5] S. Ducruix, D. Durox, S. Candel, Theoretical and experimental determinations of the transfer function of a laminar premixed flame, Proceedings of the Combustion Institute 28 (1) (2000) 765–773.
[6] T. Schuller, D. Durox, S. Candel, A unified model for the prediction of laminar flame transfer functions: Comparisons between conical and V-flame dynamics, Combustion and Flame 134 (1–2) (2003) 21–34.
[7] T. Lieuwen, Nonlinear kinematic response of premixed flames to harmonic velocity disturbances, Proceedings of the Combustion Institute 30 (2) (2005) 1725–1732.
[8] L. Boyer, J. Quinard, On the dynamics of anchored flames, Combustion and Flame 82 (1) (1990) 51–65.
[9] F. Baillot, D. Durox, R. Prud'homme, Experimental and theoretical study of a premixed vibrating flame, Combustion and Flame 88 (2) (1992) 149–152, IN1, 153–168.
[10] A.L. Birbaud, D. Durox, S. Candel, Upstream flow dynamics of a laminar premixed conical flame submitted to acoustic modulations, Combustion and Flame 146 (3) (2006) 541–552.
[11] V.N. Kornilov, K.R.A.M. Schreel, L.P.H. de Goey, Experimental assessment of the acoustic response of laminar premixed Bunsen flames, Proceedings of the Combustion Institute 31 (1) (2007) 1239–1246.
[12] N. Karimi, M.J. Brear, S.-H. Jin, J.P. Monty, Linear and non-linear forced response of a conical, ducted, laminar premixed flame, Combustion and Flame 156 (11) (2009) 2201–2212.
[13] T. Schuller, S. Ducruix, D. Durox, S. Candel, Modeling tools for the prediction of premixed flame transfer functions, Proceedings of the Combustion Institute 29 (1) (2002) 107–113.
[14] P. Auzillon, B. Fiorina, R. Vicquelin, N. Darabiha, O. Gicquel, D. Veynante, Modeling chemical flame structure and combustion dynamics in LES, Proceedings of the Combustion Institute 33 (1) (2011) 1331–1338.
[15] H.Y. Wang, C.K. Law, T. Lieuwen, Linear response of stretch-affected premixed flames to flow oscillations, Combustion and Flame 156 (4) (2009) 889–895.
[16] H.M. Altay, S. Park, D. Wu, D. Wee, A.M. Annaswamy, A.F. Ghoniem, Modeling the dynamic response of a laminar perforated-plate stabilized flame, Proceedings of the Combustion Institute 32 (1) (2009) 1359–1366.
[17] A. Cuquel, D. Durox, T. Schuller, Theoretical and experimental determination of the flame transfer function of confined premixed flames, in: 7th Mediterranean Symposium on Combustion, 2011.
[18] A.P. Dowling, A kinematic model of a ducted flame, Journal of Fluid Mechanics 394 (1) (1999) 51–72.
[19] D. Lee, T. Lieuwen, Premixed flame kinematics in a longitudinal acoustic field, Journal of Propulsion and Power 19 (2003) 837–846.
[20] Preetham, T. Lieuwen, Nonlinear flame-flow transfer function calculations: Flow disturbance celerity effects, AIAA Paper 2004-4035, 2004.
[21] Giulio Borghesi, Fernando Biagioli, Bruno Schuermans, Dynamic response of turbulent swirling flames to acoustic perturbations, Combustion Theory and Modelling 13 (3) (2009) 487–512.
[22] R. Rook, L.P.H. de Goey, L.M.T. Somers, K.R.A.M. Schreel, R. Parchen, Response of burner-stabilized flat flames to acoustic perturbations, Combustion Theory and Modelling 6 (2) (2002) 223–242.
[23] R. Rook, L.P.H. de Goey, The acoustic response of burner-stabilized flat flames: A two-dimensional numerical analysis, Combustion and Flame 133 (1–2) (2003) 119–132.

[24] X.J. Gu, M.Z. Haq, M. Lawes, R. Woolley, Laminar burning velocity and Markstein lengths of methane/air mixtures, Combustion and Flame 121 (1–2) (2000) 41–58.
[25] I.R. Hurle, R.B. Price, T.M. Sugden, A. Thomas, Sound emission from open turbulent premixed flames, Proceedings of the Royal Society of London. Series A. Mathematical and Physical Sciences 303 (1475) (1968) 409–427.
[26] Kushal S. Kedia, Ahmed F. Ghoniem, Mechanisms of stabilization and blowoff of a premixed flame downstream of a heat-conducting perforated plate, Combustion and Flame 159 (3) (2012) 1055–1069.